

## Aldol Condensations Over Reconstructed Mg–Al Hydrotalcites: Structure–Activity Relationships Related to the Rehydration Method

Sònia Abelló,<sup>[a]</sup> Francesc Medina,<sup>\*[a]</sup> Didier Tichit,<sup>[b]</sup> Javier Pérez-Ramírez,<sup>[c]</sup> Johan C. Groen,<sup>[d]</sup> Jesús E. Sueiras,<sup>[a]</sup> Pilar Salagre,<sup>[a]</sup> and Yolanda Cesteros<sup>[a]</sup>

**Abstract:** Two different rehydration procedures in the liquid or gas phase have been applied to reconstruct mixed oxides derived from calcined hydrotalcite-like materials to be used as catalysts for aldol condensation reactions. The as-synthesized hydrotalcite, its decomposition product, as well as the reconstructed solids upon rehydration were characterized by XRD, N<sub>2</sub> adsorption, He pycnometry, FTIR, SEM, TEM, <sup>27</sup>Al MAS-NMR and CO<sub>2</sub>-TPD (TPD = temperature-programmed desorption). Compared to the Mg–Al mixed oxide rehydrated in the gas phase (HT-rg), that rehydrated in the liquid phase (HT-rl) exhibits a superior catalytic performance with respect to the aldol condensation of citral with ketones to yield pseudoionones and in

the self-aldolization of acetone. The textural properties of HT-rl and HT-rg differ strongly and determine the catalytic behavior. A memory effect led to a higher degree of reconstruction of the lamellar structure when the mixed oxide was rehydrated in the gas phase rather than in the liquid phase, although liquid-phase rehydration under fast stirring produced a surface area that was 26 times greater. This contrasts to typical statements in the literature claiming a higher degree of reconstruction in the presence of large amounts of water in the medium. CO<sub>2</sub>-TPD

shows that the number of OH<sup>−</sup> groups and their nature are very similar in HT-rg and HT-rl, and cannot explain the markedly different catalytic behavior. Accordingly, only a small fraction of the available basic sites in the rehydrated samples is active in liquid-phase aldol condensations. Our results support the model in which only basic sites near the edges of the hydrotalcite platelets are partaking in aldol reactions. Based on this, reconstructed materials with small crystallites (produced by exfoliation during mechanical stirring), that is, possessing a high external surface area, are beneficial in the reactions compared to larger crystals with a high degree of intraplatelet porosity.

**Keywords:** rehydration · aldol reaction · layered compounds · memory effect · stirring speed

### Introduction

In recent years, hydrotalcite-like compounds (HTlcs) have been used in numerous reactions and applications, such as catalyst precursors or supports, ion-exchangers, stabilisers and adsorbents.<sup>[1–3]</sup> These materials are layered double hydroxides with the general formula  $[M^{2+}_n M^{3+}_m (OH)_{2(n+m)}]^{m+} [A^{x-}]_{m/x} y H_2O$ , where M<sup>2+</sup> and M<sup>3+</sup> are divalent and trivalent metal cations, respectively, A represents the x-valent anion (typically carbonate) required to compensate the net positive charge of the brucite-like layers, and y is the number of water molecules in the interlayer space. The ratio  $m/(m+n)$  may vary from 0.17 to 0.33, depending on the particular combination of divalent and trivalent metals.

Thermal decomposition of Mg–Al HTlcs leads to a well-dispersed mixture of magnesium and aluminium oxides (MgAlO). These mixed oxides show a memory effect, a

[a] S. Abelló, Dr. F. Medina, Dr. J. E. Sueiras, Dr. P. Salagre, Dr. Y. Cesteros  
Dept. de Química i Enginyeria Química, Universitat Rovira i Virgili, 43007, Tarragona (Spain)  
Fax: (+34) 977-559-621  
E-mail: fmedina@etse.urv.es

[b] Dr. D. Tichit  
Laboratoire des Matériaux Catalytiques et Catalyse en Chimie Organique, UMR 5618 CNRS-ENSCM  
8 rue de L'École Normale, 34296 Montpellier Cedex 5 (France)

[c] Dr. J. Pérez-Ramírez  
Yara Technology Centre Porsgrunn, Catalysis and Nitric Acid Technology  
P.O. Box 2560, N-3908, Porsgrunn (Norway)

[d] J. C. Groen  
Applied Catalyst Characterization, DelftChemTech, Delft University of Technology  
Julianalaan 136, 2628 BL, Delft (The Netherlands)

property by which they can recover the original lamellar structure if they come into contact with water vapour or are immersed in water under a decarbonated atmosphere. This leads to meixnerite (magnesium aluminium hydroxide hydrate), that is, HTlc intercalated with  $\text{OH}^-$  as compensating anions in the interlayer.<sup>[4]</sup> These rehydrated materials have been applied to a number of base-catalysed reactions on account of their Brønsted basic character.<sup>[5–7]</sup> Applications include self- and cross-aldol condensation of aldehydes and ketones,<sup>[8–11]</sup> Knoevenagel and Claisen–Schmidt condensations,<sup>[12–14]</sup> Michael additions,<sup>[15]</sup> etc.

It has been clearly established that the precalcination temperature is a determining parameter governing the reconstruction, which is complete when the formation of a spinel-like phase, for example,  $\text{MgAl}_2\text{O}_4$  in case of Mg–Al HTlc, is avoided. Reconstruction cannot be completed if this phase has been formed, even after several days of rehydration.<sup>[16,17]</sup>

The catalytic performance of reconstructed HTlcs as a function of the rehydration procedure applied is not well-understood. Corma and co-workers<sup>[18,19]</sup> approached this aspect by carrying out the rehydration of calcined Mg–Al hydrotalcite in a stream of nitrogen saturated with water vapour (gas-phase rehydration), or, alternatively, by adding water directly to the calcined material (liquid-phase rehydration). Both samples, which had a very similar level of regeneration with regard to the layered structure according to XRD, displayed practically the same activity in the condensation reactions of citral and acetone or methyl ethyl ketone.<sup>[19]</sup> However, in the condensation reaction of citral and methyl ethyl ketone, a higher selectivity for methylpseudoionones was obtained with the gas-phase rehydrated sample, which suggests a comparatively larger ratio of Brønsted to Lewis basic sites in the latter sample compared to the liquid-phase rehydrated sample.

Experiments that employed the two types of rehydration procedure over decomposed Mg–Al HTlc have also been performed by de Jong and co-workers.<sup>[20–22]</sup> In these studies, rehydration in water vapour led to a lower crystallinity and specific surface area than rehydration by immersion (57 versus  $200 \text{ m}^2 \text{ g}^{-1}$ ). The as-synthesized hydrotalcites displayed specific surface areas in the range of  $90\text{--}100 \text{ m}^2 \text{ g}^{-1}$ . A similar observation was also reported by Figueras et al.,<sup>[10,23–25]</sup> the surface area of the mixed oxide ( $95 \text{ m}^2 \text{ g}^{-1}$ ) decreased to  $20 \text{ m}^2 \text{ g}^{-1}$  after rehydration of the sample in the vapour phase, which led to a restoration of the layered structure. According to these authors, this accounted for a limitation of the rehydration process by the diffusion of water within the particles, and the surface corresponds to the external area of the crystals.

These features suggest that the rehydration process of the crystallites is certainly a key parameter governing the number and the strength of active  $\text{OH}^-$  sites in base-catalysed reactions. Accordingly, the present study was undertaken to derive structure–activity relationships in differently reconstructed Mg–Al-HTlcs for various aldol condensation reactions, such as citral and acetone or 2-butanone, to

obtain pseudoionone or methyl-pseudoionone, respectively, and in the self-aldolization of acetone.

## Results and Discussion

### Material characterization

**Chemical composition:** Analysis of the as-synthesized sample, HT-as, by inductively coupled plasma (ICP) spectrometry as well as by thermogravimetry (TG) revealed the following chemical composition:  $[\text{Mg}_{0.777}\text{Al}_{0.223}(\text{OH})_2] \cdot (\text{CO}_3)_{0.113} \cdot 0.575 \text{H}_2\text{O}$ , indicating the good agreement between the nominal ratio in the liquid and the actual ratio in the solid. The amount of sodium in the as-synthesized hydrotalcite was less than 0.1 wt%, indicating that washing of the solid after filtration was effective. Furthermore, nitrogen was not detected by elemental analysis.

**X-ray diffraction:** Figure 1 shows the XRD patterns of the as-synthesized Mg–Al hydrotalcites (HT-as), calcined hydrotalcite (HT-c), rehydrated hydrotalcite in the gas phase

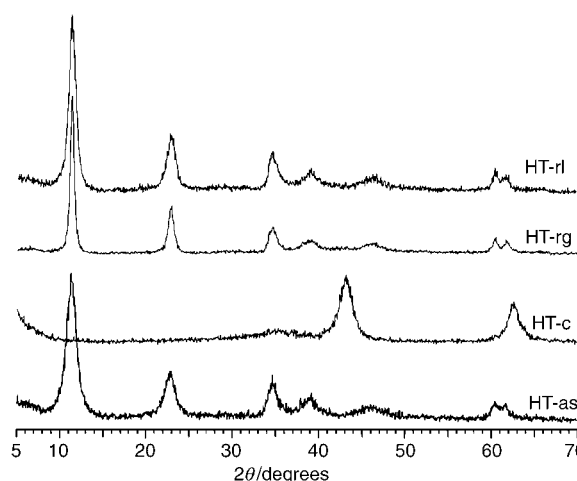


Figure 1. X-ray diffraction patterns of the materials investigated in this study.

(HT-rg) and rehydrated hydrotalcite in the liquid phase (HT-rl) (at 500 rpm for 1 h). The as-synthesized sample shows a pure hydrotalcite phase (JCPDS 22-700). Upon calcination of the material at 723 K, the layered structure was destroyed and a mixed oxide phase  $\text{Mg}(\text{Al})\text{O}_x$  was obtained, corresponding to the periclase structure (JCPDS 87-0653). After calcination and intercalation of  $\text{OH}^-$  ions by rehydration in the gas and liquid phases, the original layered structure was recovered, which corresponded to meixnerite (JCPDS 35-0965). However, the XRD pattern of HT-rl shows broader peaks than that of HT-rg, indicating a lower crystallinity, namely as a consequence of the lower crystallite size in the former sample (see microscopy). This can be tentatively attributed to the effect of mechanical stirring

during the rehydration process in the liquid phase, which can break and exfoliate the hydrotalcite-like platelets to increase the surface area of the solid, and/or to the mechanism of water diffusion in the galleries.

**N<sub>2</sub> adsorption:** N<sub>2</sub> adsorption experiments were performed to derive detailed information on pore size distributions. Upon calcination of HT-as, the porosity substantially increases leading to a more pronounced hysteresis loop in the isotherm of HT-c (Figure 2), which indicates formation of extra (meso)porosity. This result is supported by the higher surface area and total pore volume in HT-c (210 m<sup>2</sup> g<sup>-1</sup>) compared to HT-as (57 m<sup>2</sup> g<sup>-1</sup>) (Table 1). In addition, formation of some microporosity in HT-c can also be concluded.

Application of the BJH model to the adsorption branch of the isotherm further indicates that thermal decomposition

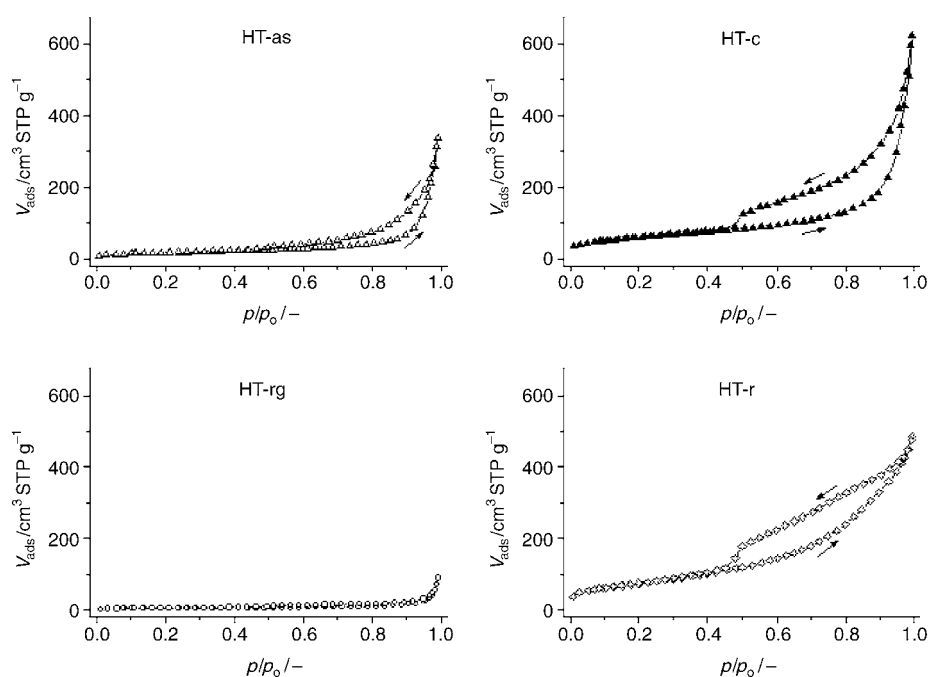


Figure 2. N<sub>2</sub> adsorption isotherms of the different samples.

Table 1. Textural and chemical properties of the materials.

Sample	$S_{\text{BET}}^{[a]}$ [m <sup>2</sup> g <sup>-1</sup> ]	$S_{\text{meso}}^{[b]}$ [m <sup>2</sup> g <sup>-1</sup> ]	$V_{\text{micro}}^{[b]}$ [cm <sup>3</sup> g <sup>-1</sup> ]	$V_{\text{p}}^{[c]}$ [cm <sup>3</sup> g <sup>-1</sup> ]	$\rho_{\text{He}}^{[d]}$ [g cm <sup>-3</sup> ]	$H^{[e]}$ [%]	$C^{[e]}$ [%]
HT-as	57	57	0.00	0.4	1.93	4.04	1.79
HT-c	210	180	0.01	0.8	2.73	0.88	0.35
HT-rg	15	15	0.00	0.1	2.15	4.36	0.49
HT-rl	270	270	0.00	0.7	2.56	3.24	1.03

[a] BET method. [b] t method. [c] Volume at  $p/p_0 = 0.99$ . [d] He pycnometry. [e] Elemental analysis.

of the as-synthesized hydrotalcite induces the development of additional porosity covering a broad range of pore sizes, with a maximum at ~50 nm.

Interestingly, the pore-size distribution in HT-c is similar to that in HT-as (Figure 3). This led to the conclusion, in

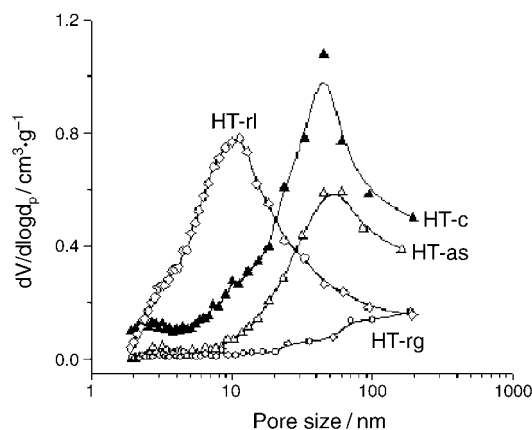


Figure 3. BJH pore size distribution derived from the adsorption branch of the N<sub>2</sub> adsorption isotherms.

particular, that the smaller mesopores which have been created extend into lower pore sizes. It is thought that these lower pore sizes are probably responsible for the significant increase in BET surface area. This porosity development upon calcination is in agreement with results previously reported by de Jong and co-workers.<sup>[21]</sup>

Rehydration in the liquid or gas phases leads to remarkable differences in the porous characteristics of the obtained material. The sample rehydrated in the gas phase (HT-rg) does not show a significant porosity, but has a low BET surface area (15 m<sup>2</sup> g<sup>-1</sup>) and pore volume (0.1 cm<sup>3</sup> g<sup>-1</sup>). A similar but less dramatic decrease in the BET surface area (from 253 to 57 m<sup>2</sup> g<sup>-1</sup>) was observed in reference [21], and possibly results from slightly different rehydration conditions. Contrarily, rehydration in the liquid phase (HT-rl) leads to a remarkable BET surface area of 270 m<sup>2</sup> g<sup>-1</sup>, which is even higher than the surface area of the calcined material, whereas the pore volume of HT-rl is slightly lower than

in the calcined material. This result suggests a markedly different porous structure for both materials, as confirmed by the BJH pore size distribution in Figure 3, which shows that the majority of pores are smaller than 50 nm with a distribution centered at ~10 nm, without any appreciable micro-

porosity. Although no details were provided by de Jong and co-workers<sup>[20]</sup> on the pore size evolution upon rehydration of Mg–Al HTlc in the liquid phase, the increase in surface area accompanied by a decreased pore volume suggests a similar change in the porous characteristics.

The difference in the porous characteristics of the liquid-phase rehydrated material could be produced by exfoliation of the meixnerite crystals during the mechanical stirring. This was investigated in additional experiments by changing the stirring speed and the rehydration time (Table 2); however, the same magnet was always used.

Table 2. Effect of the stirring speed and time over rehydrated hydrotalcites.

Sample	Rehydration time [h]	Stirring speed [rpm]	$S_{\text{BET}}^{[a]}$ [ $\text{m}^{-2}\text{g}^{-1}$ ]	Reconstruction <sup>[b]</sup> [%]
HT-rl-100	1	100	203	66
HT-rl-300	1	300	229	74
HT-rl	1	500	270	83
HT-rl-700A	1	700	374	89
HT-rl-700B	0.16	700	241	67
HT-rl-700C	6	700	401	92

[a] BET method. [b] Calculated by TGA.

As expected, a higher surface area for the rehydrated materials was observed when the stirring speed was increased from 100 to 700 rpm. This can be explained by the higher degree of exfoliation obtained by the rupture of particles. When a stirring speed of 700 rpm was used with different rehydration times, the same effect was detected.

Helium pycnometry (Table 1) provides information on the real (skeleton) density of the material, independently of the accessible porosity. As expected, the density of the calcined material ( $2.73 \text{ g cm}^{-3}$ ) is much higher than that of the as-synthesized hydrotalcite ( $1.93 \text{ g cm}^{-3}$ ). The density of the rehydrated hydrotalcites presents important differences: it is higher in HT-rl ( $2.56 \text{ g cm}^{-3}$ ) than in HT-rg ( $2.15 \text{ g cm}^{-3}$ ). This fact can be explained taking into account the structure of the reconstructed hydrotalcites. If the rehydration procedures would lead to total reconstruction, HT-rl and HT-rg should possess a very similar density to HT-as. However, the densities obtained in the rehydrated hydrotalcites lie between those of HT-as and HT-c, which strongly suggests that the layered structure was partially recovered. That the density in HT-rg ( $2.15 \text{ g cm}^{-3}$ ) is lower than that in HT-rl (Table 1) indicates a more efficient reconstruction in the gas-phase rehydrated sample, in agreement with the results of XRD and other techniques described below. In contrast to a previous hypothesis,<sup>[24]</sup> this indicates that the diffusion of water within the particles is not the limiting factor of the rehydration process. The low surface area of HT-rg is probably caused by steric hindrance produced by the  $\text{OH}^-$  and water molecules in the interlayer space.

**Thermogravimetric analysis:** Figure 4 shows the thermogravimetric analysis of the as-synthesized and rehydrated sam-

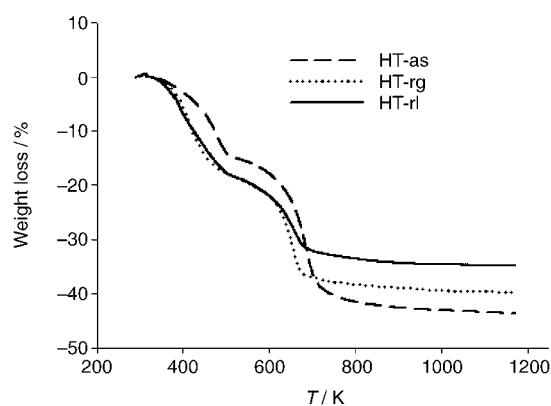


Figure 4. Thermogravimetric analysis of the as-synthesized and rehydrated hydrotalcites.

ples. The decomposition profiles are in good agreement with those in the literature for hydrotalcite-like compounds,<sup>[26,27]</sup> with a total weight loss in the range of 34–45%. Similar behavior was observed for the three samples, with two distinct weight-loss processes. The first weight loss at temperatures below 473 K is attributed to the loss of physically adsorbed and interlayer water molecules, whereas the second weight loss (473–773 K) originates from the dehydroxylation of the brucite-like sheets and decomposition of carbonates in the interlayer. The first weight loss of  $\approx 18\%$  for the rehydrated samples is similar in both cases. However, the second weight loss was 5% higher in HT-rg (21.7%) than in HT-rl (16.8%). This indicates a similar amount of water molecules, but an increase of compensating  $\text{OH}^-$  ions between the brucite-like sheets of the sample rehydrated in the gas phase compared to that rehydrated in the liquid phase. This nicely indicates that the degree of rehydration in the gas phase is higher than in the liquid phase. Accordingly, the degree of reconstruction was estimated to be 94% in HT-rg and 83% in HT-rl. These results are in agreement with the C and H elemental analysis of the samples in Table 1 that show a 4.36 wt% and 3.24 wt% of hydrogen for HT-rg and HT-rl, respectively. The carbon content in the samples indicates that not all the carbonates are decomposed during the calcination process. Furthermore, the increase in the amount of carbon detected in HT-rl, indicates a major contamination with  $\text{CO}_2$  during rehydration in liquid phase.

**IR spectroscopy:** Figure 5 shows the IR spectra of the dried samples. The FTIR spectra of various hydrotalcite-like materials have been widely discussed elsewhere.<sup>[3,28–33]</sup> The spectrum of HT-as exhibits a typical broad band at  $3471 \text{ cm}^{-1}$ , which is attributed to the stretching mode of hydrogen-bonded hydroxy groups from the brucite-like layers and interlayer water. The shoulder at  $\approx 3000 \text{ cm}^{-1}$  is assigned to hydrogen bonding between water and carbonate in the interlayer, whereas the band at  $1643 \text{ cm}^{-1}$  is the  $\text{H}_2\text{O}$  bending vibration. The vibration of the carbonates (asymmetric stretching,  $\nu_3$ ) appears at  $1374 \text{ cm}^{-1}$  and could be assigned to interlayer carbonates (chelating or bridging biden-

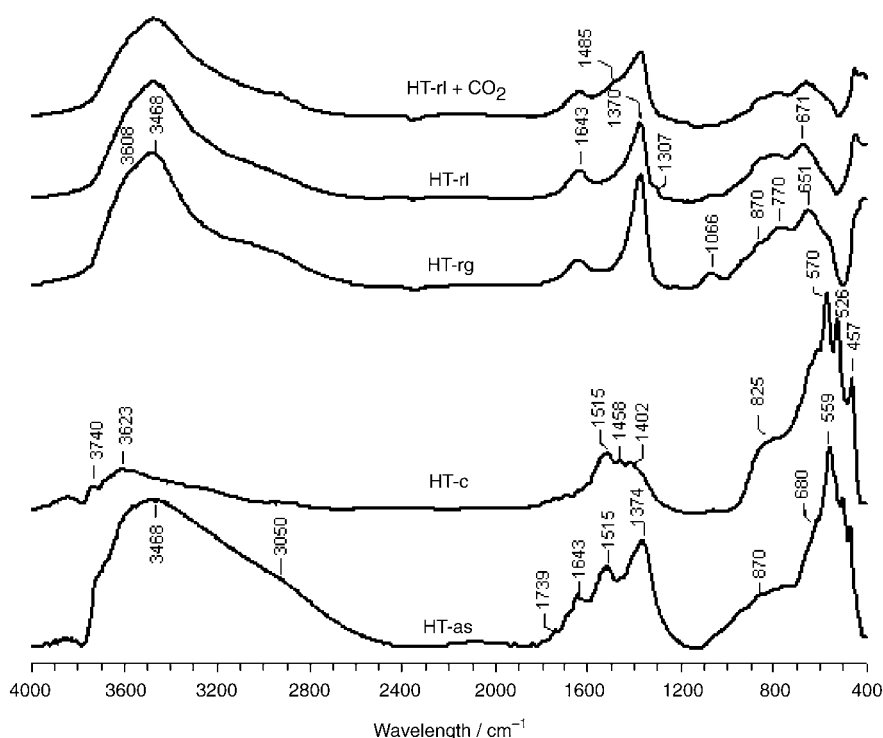


Figure 5. Fourier-transform infrared spectra of the different samples.

tate). The vibration at  $1515\text{ cm}^{-1}$  is ascribed to a reduction in the symmetry caused by the presence of monodentate carbonates ( $\nu_{\text{asym}}$  O-C-O) interacting with  $\text{Mg}^{2+}$ , as reported elsewhere,<sup>[3,29–30]</sup> whereas the band at  $1740\text{ cm}^{-1}$  is the bending mode of water. The low frequency region shows a band at about  $560\text{ cm}^{-1}$ , corresponding to the translation modes of hydroxy groups, influenced by  $\text{Al}^{3+}$  cations. The band at  $870\text{ cm}^{-1}$  is characteristic for the out-of-plane deformation of carbonate ( $\nu_2$ ), whereas the in-plane bending is located at  $680\text{ cm}^{-1}$  ( $\nu_4$ ). Calcination of this material (Figure 5, HT-c) shows that water has been virtually removed (see C and H analysis in Table 1) because of the disappearance of the bands at  $1643$  (corresponding to the water bending vibration),  $1739$  (water bending vibration restricted in the interlayer) and  $3050\text{ cm}^{-1}$  (interaction  $\text{H}_2\text{O}-\text{CO}_3^{2-}$  in the interlayer). The intensity of the band at about  $3470\text{ cm}^{-1}$  also decreases by dehydroxylation. The carbonate band suffers from a rearrangement in the interlamellar space, the band at  $1374\text{ cm}^{-1}$  decreases in intensity and two peaks at about  $1515$  and about  $1400\text{ cm}^{-1}$  are observed because of the interaction between  $\text{CO}_3^{2-}$  and  $\text{Mg}^{2+}$ . The band at  $1458\text{ cm}^{-1}$  is attributed to the adsorbed carbonate upon thermal decomposition. It can be concluded that the applied calcination temperature is not sufficient to completely eliminate hydroxyls and carbonates, although the hydrotalcite phase is destroyed. This fact is in agreement with the results in Table 1, which show  $0.35\text{ wt}\%$  and  $0.88\text{ wt}\%$  of carbon and hydrogen, respectively, in the calcined sample. The bands below  $1000\text{ cm}^{-1}$  are the vibration modes for Mg–O and Al–O in the mixed oxide formed.<sup>[32]</sup> The band at  $457\text{ cm}^{-1}$  is at-

tributed to the vibrations of the  $\text{MgO}$  and  $\text{Al}_2\text{O}_3$ . Exposure of the calcined sample to a flow of wet gas (HT-rg in Figure 5) induces a recovery of the hydrotalcite-like structure. The same effect occurs when the calcined sample is rehydrated in the liquid phase (HT-rl in Figure 5). The bands at  $3050$  and  $1640\text{ cm}^{-1}$  reappear in both cases, showing a significantly larger amount of water molecules when rehydration is carried out in the gas phase. This means that the reconstruction of the hydrotalcite-like structure is greater than in the liquid phase. In the high-energy region, a band at  $634\text{ cm}^{-1}$  is present and could be assigned to the Mg–OH translation.<sup>[32]</sup> The bands at  $770$  and  $1066\text{ cm}^{-1}$  can be assigned to the translation and deformation modes respectively, of the hydroxy groups influenced by the  $\text{Al}^{3+}$

ions. The band at  $1370\text{ cm}^{-1}$ , which is recovered as a symmetric peak, corresponds also to interlayer carbonate (mainly bidentate carbonates),<sup>[30]</sup> indicating that a significant amount of carbonates is still present after calcination/rehydration (probably, by introduction of  $\text{CO}_3^{2-}$  in the recovery process). This result is in agreement with C,H analysis (Table 1): where the amount of carbon and hydrogen and is  $1.03\text{ wt}\%$  and  $3.24\text{ wt}\%$ , respectively, in HT-rl and  $0.49\text{ wt}\%$  and  $4.36\text{ wt}\%$ , respectively, in the HT-rg samples. Figure 5 also shows the spectrum of the liquid-phase rehydrated sample after  $\text{CO}_2$  adsorption at  $353\text{ K}$  (HT-rl- $\text{CO}_2$  in Figure 5), under the same conditions as the  $\text{CO}_2$ -TPD (TPD=temperature-programmed desorption) experiments. The only difference between this latter sample and HT-rl is the shoulder at about  $1485\text{ cm}^{-1}$ , which is assigned to the symmetric O-C-O stretching mode of bicarbonate anions. When  $\text{CO}_2$  is adsorbed on a base and at pH values up to 8,  $\text{CO}_3^{2-}$  formation is more favourable than  $\text{HCO}_3^-$  formation.<sup>[34]</sup> Accordingly, before adsorption of  $\text{CO}_2$ , a rehydrated sample shows a carbonate peak because only stronger basic sites are evaluated. After  $\text{CO}_2$  adsorption, bicarbonates result from remaining weaker  $\text{OH}^-$  groups.

**Scanning electron microscopy:** SEM images were recorded to investigate the morphology of the different samples (Figure 6). The micrograph of the as-synthesized hydrotalcite shows a well-developed layered structure. The mixed oxide obtained upon calcination at  $723\text{ K}$  maintains the lamellar structure and the morphology seems to be similar to that of HT-as. When rehydration was performed in the

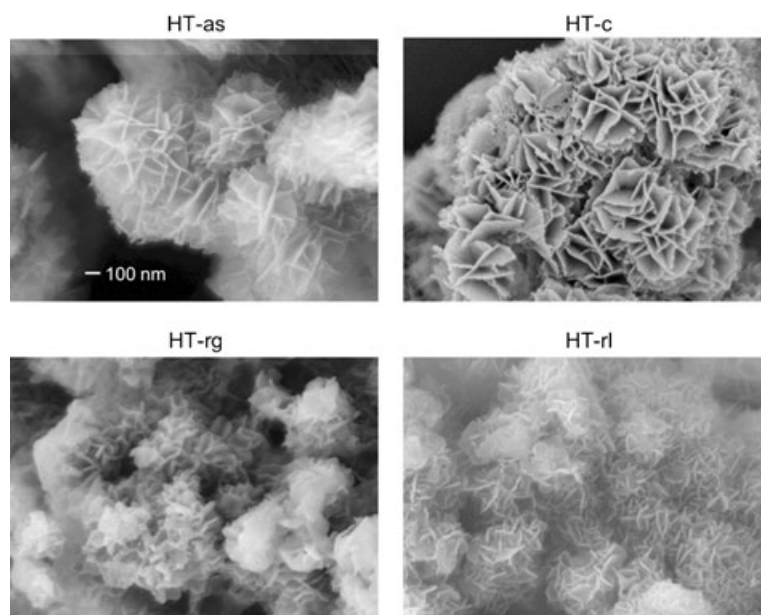


Figure 6. Scanning electron micrographs of the as-synthesized and rehydrated hydrotalcites.

liquid phase, a sample with a high degree of exfoliation was obtained, as mentioned above. The shape is preserved with respect to the as-synthesized material, and the smaller particles generated by mechanical stirring in the rehydration procedure formed very thin platelets. Contrarily, HT-rg is built of complex aggregates of hydrotalcite platelets that are significantly thicker than those in HT-rl. This is in agreement with the higher crystallinity (XRD) and markedly lower surface area ( $N_2$  adsorption) of HT-rg.

**Transmission electron microscopy:** HRTEM was performed to obtain further information on the different morphologic features of the samples (Figure 7). The results are in agreement with those obtained by other characterization techniques. In the calcined sample (HT-c), clearly discernible platelets are shown. This suggests that the platelet morphology does not collapse, even if the layered hydrotalcite structure is no longer present. HT-rg presents much thicker platelets than HT-rl, indicating a relatively high degree of sintering in the former sample. Moreover, the micrographs suggest a better reconstruction of the lamellar phase in HT-rg than in HT-rl (see also Figure 8). The crystalline phase is observed over a much wider range, which is in agreement with our previous observations.

**Nuclear magnetic resonance of  $^{27}\text{Al}$ :** The as-synthesized sample shows the majority of Al in octahedral positions, as evidenced by the signal at  $\delta \approx 10$  ppm in Figure 9. The small contribution at  $\delta \approx 80$  ppm is attributed to a spinning side band. Upon calcination, the contribution of tetrahedrally coordinated Al increases at the expense of the octahedrally coordinated Al, correlating with the collapse of the lamellar structure. Rehydration in both liquid and gas phases shows a partial recovery of the initial as-synthesized pattern, sug-

gesting that the (partial) reconstruction of the HTlc structure, which (based on the signal intensities) is less complete in HT-rl ( $\text{Al}_{\text{Oh}}/\text{Al}_{\text{Td}} = 3.9$ ) than in HT-rg ( $\text{Al}_{\text{Oh}}/\text{Al}_{\text{Td}} = 4.4$ ), in good agreement with the TGA and XRD results.

**Temperature-programmed desorption of  $\text{CO}_2$ :**  $\text{CO}_2$ -TPD is typically applied to determine the density and strength of basic sites in mixed oxides derived from the calcination of hydrotalcites.<sup>[35–37]</sup> To establish a correlation between the catalytic activity and the textural and basic properties, experiments were carried out over both rehydrated samples. From the TPD of  $\text{CO}_2$  in Figure 10, two peaks were identified indicating

that two types of basic sites can be distinguished in the rehydrated Mg–Al mixed oxides. The main peak is centered around 673–693 K, whereas the other one has its maximum at  $\approx 823$  K. The total number of basic sites is higher ( $803.9 \mu\text{mol g}_{\text{cat}}^{-1}$ ) when rehydration is carried out in the

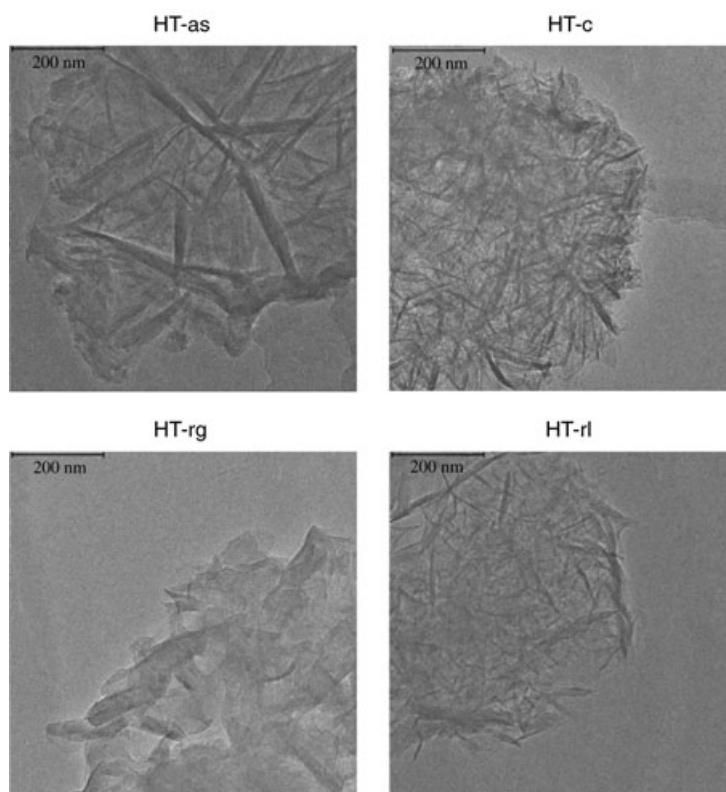


Figure 7. Low-magnification transmission electron micrographs of the as-synthesized and rehydrated hydrotalcites.

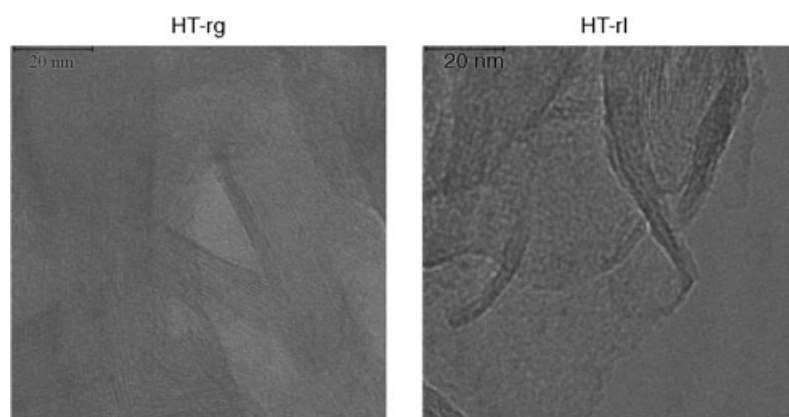


Figure 8. High-magnification transmission electron micrographs of the rehydrated hydrotalcites.

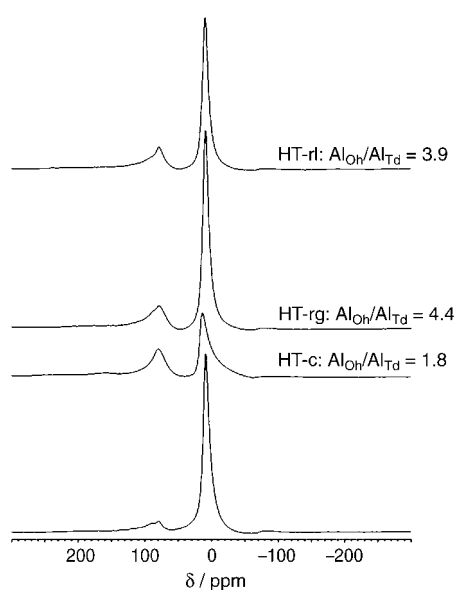


Figure 9.  $^{27}\text{Al}$  MAS-NMR spectra of the as-synthesized, calcined, and rehydrated samples.

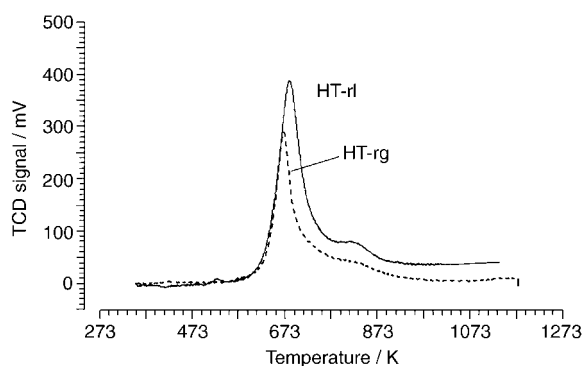


Figure 10.  $\text{CO}_2$  uptake during temperature-programmed desorption experiments over the rehydrated hydrotalcites.  $\text{CO}_2$  adsorption at 353 K for 1 h.

liquid phase (HT-rl) than when it is carried out in the gas phase (HT-rg) ( $437.7 \mu\text{mol g}_{\text{cat}}^{-1}$ ). Based on the  $\text{CO}_2$  profiles, the basic nature of the  $\text{OH}^-$  ions appears to be similar in HT-rl and HT-rg, but the number of basic sites in HT-rl is double that in HT-rg (Table 2). The contribution of the smaller peak with respect to the total number of basic sites is about 20% in both cases. The  $\text{CO}_2$  uptake results from different types of carbonate coordination in the interlayer space. In this sense, different species have been identified, such as mono-

dentate, bidentate, or bicarbonate anions. Monodentate and bidentate carbonate formation involves low-coordinate oxygen anions, which are in turn thus strong basic sites.<sup>[38,39]</sup> Bicarbonate requires surface hydroxy groups. We suggest that the first peak, which decomposes at temperatures of about 700 K, can be attributed to the contribution of mainly bidentate carbonates, together with bicarbonate species, on the catalyst surface, whereas the smaller peak above 800 K is attributable to monodentate species. This result is in agreement with our FT-IR results. Taking into account the TGA results and comparing the amount of  $\text{OH}^-$  with the amount of  $\text{CO}_2$  desorbed (Table 2), the proportion of basic sites detected by the  $\text{CO}_2$  molecules is approximately 13% and 30% for HT-rg and HT-rl, respectively, despite the higher degree of reconstruction, and thus the higher number of  $\text{OH}^-$  groups in HT-rg (see Figure 4). This indicates that 1) not all of the total  $\text{OH}^-$  groups are probed by  $\text{CO}_2$  molecules and 2) the  $\text{OH}^-$  groups in the HT-rl sample are more accessible (owing to the higher porosity and specific surface area). Under our experimental conditions, it is probable that the  $\text{OH}^-$  ions probed by  $\text{CO}_2$  are located at the edges of the platelets. From the quantification in Table 3, the  $\text{CO}_2$  adsorption with respect to the bulk Al content shows that approximately 11.6% and 24.5% of the  $\text{OH}^-$  sites, for HT-rg and HT-rl, respectively, are also evaluated.

Table 3. Quantification of the  $\text{CO}_2$ -TPD profiles for the rehydrated hydrotalcites.

Sample	Peak at 693 K [%]	Peak at 823 K [%]	Total $\text{CO}_2$ evolved [ $\mu\text{mol g}^{-1}$ ]	$\text{CO}_2/\text{Al}$ ratio <sup>[a]</sup>
HT-rg	80	20	438	0.116 (0.023) <sup>[b]</sup>
HT-rl	78	22	804	0.245 (0.054) <sup>[b]</sup>

[a] Mol of total adsorbed  $\text{CO}_2$  per mol of Al in the HT. [b] Between brackets, contribution of peak at 823 K.

These results are in fair agreement with those determined from thermogravimetric analysis. The higher accessibility shown by the HT-rl sample could be explained by the fact

that it has approximately 18 times more surface area than HT-rg (Table 1). Taking into account the higher  $S_{\text{BET}}$  of HT-rl, the difference in basicity is just incremental. This is strong evidence that only the edges of the platelets are operative, namely, the active sites in aldol condensations (see the section on structure–activity relationships). Therefore, intuitively there are two factors that are related: porosity and crystal size, although it seems that the relatively small crystal size is the activity-directing factor in these reactions. In accordance with these results, Figure 11 shows a representative structure that highlights the main differences between HT-rg and HT-rl.

### Catalytic performance

It is well known that the first step in the aldol condensation reaction is the extraction of a proton from the  $\alpha$ -carbon atom of a ketone/aldehyde by a basic site of the catalyst to generate a reactive enolate. The nucleophilic enolate attacks the carbonyl group of the substrate to produce an intermediate alkoxide. Subsequently, the alkoxide deprotonates a water molecule, and thus creates a hydroxide and a  $\beta$ -hydroxyaldehyde or aldol product. After that and depending on the reaction conditions, a dehydration process may occur to yield the final conjugated aldehyde.

In this sense, materials obtained from hydrotalcite-like compounds, which show both Lewis and Brønsted basic sites, are efficient in this type of reactions. This work examines aldol condensations between citral and acetone or citral and methyl ethyl ketone (MEK), as well as the self-aldolization of acetone over reconstructed hydrotalcite-like materials. A simplified scheme for these reactions is represented in Scheme 1. Preliminary tests with HT-as and HT-c in the condensation reaction between citral and acetone at 333 K have shown virtually no activity over these catalysts over a period of 24 h. These materials mainly contain Lewis basic sites, which are inactive in the reaction. Rehydration of HT-c leads to a certain degree of conversion, whose absolute value strongly depends on the rehydration procedure applied. This fact is in agreement with the data reported in the literature where, for the self-condensation of acetone, the meixnerite obtained by rehydration of Mg–Al mixed oxides, is more active than its hydroxycarbonate precursors (hydrotalcites).<sup>[4]</sup> It seems that Brønsted

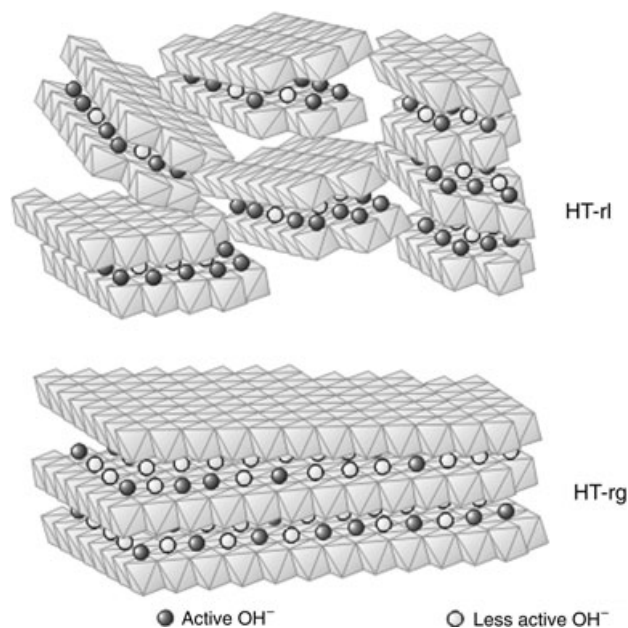
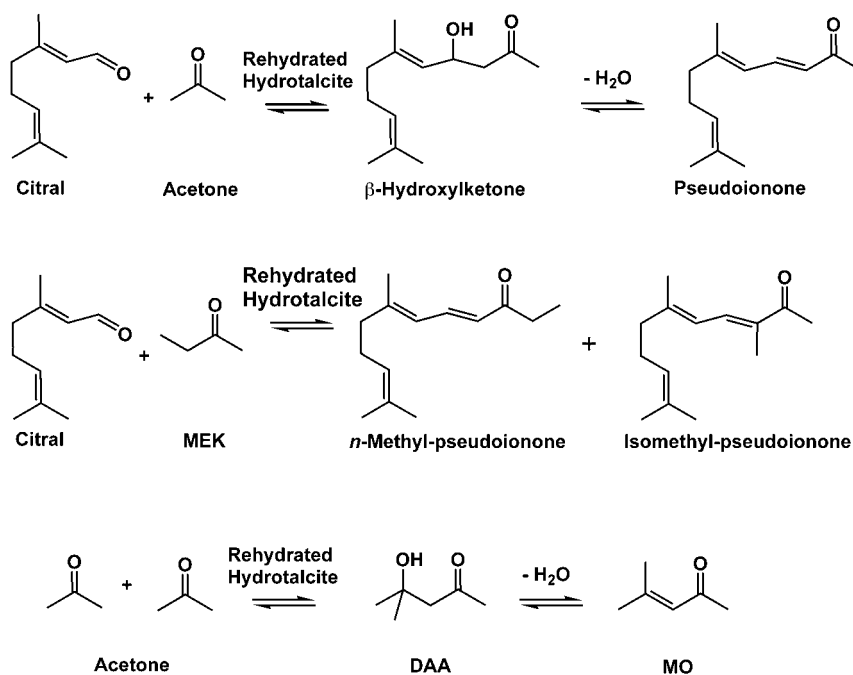


Figure 11. Schematic representation of the different reconstruction mechanism in HT-rl and HT-rg based on physico-chemical characterization results.



Scheme 1. Reactions in the aldol condensation between citral and acetone and aldolization of acetone.

ed basic  $\text{OH}^-$  ions sites play a vital role in this type of reactions.

**Influence of the rehydration procedure:** Figure 12 shows the conversion versus reaction time for HT-rg and HT-rl catalysts for the citral/acetone and citral/methyl ethyl ketone

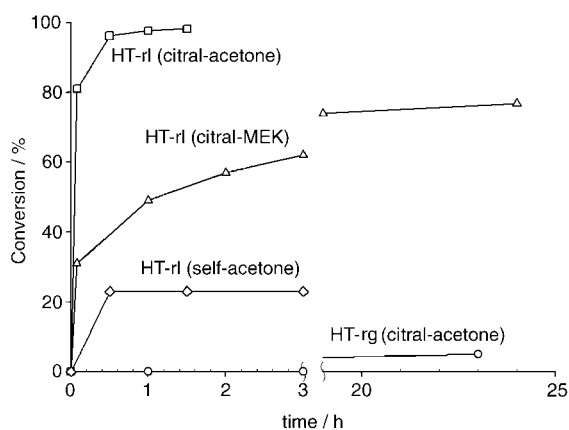


Figure 12. Conversion versus time for the reaction of citral/acetone at 333 K, citral/MEK at 333 K, and self-aldolization of acetone at 273 K over the rehydrated hydrotalcites.

(MEK) reactions and the self-condensation of acetone to diacetone alcohol (DAA). A molar ketone/citral ratio of 4.4:1 was used, and the main products for the aldol reaction between acetone and citral were a mixture of *cis*- and *trans*-pseudoionone. No  $\beta$ -hydroxyketone was observed under these reaction conditions. The aldol reaction between citral and MEK provided four isomers arising from the double attack of the two carbanions of MEK. The selectivity of the desired products of these reactions was always higher than 95%.

As mentioned above, two types of solid can be obtained according to the different rehydration procedures of the calcined hydrotalcites: HT-rl (by immersion in decarbonated liquid water at a stirring speed of 500 rpm for 1 h, and washing with ethanol) and HT-rg (by contacting with a flow of argon saturated with water vapour). For the gas-phase rehydrated samples, the flow was maintained for 10, 15, and 48 h, to obtain solids with differing amounts of water. The loss of water detected by TGA was 29, 39, and 41 wt%, respectively. The best result was achieved over the HT-rg sample containing approximately 39% water that gave a conversion of 4.3% in 1 h and 8.7% after 2.5 h in the self-aldolization of acetone. These results are not in agreement with those previously reported (23% of conversion at 273 K in 1–3 h).<sup>[8]</sup> This could be explained by the lower surface areas achieved under our rehydration conditions in the gas phase. Furthermore, other previous results with gas-phase rehydrated hydrotalcites in this kind of reactions showed that the presence of alkali metal ions (sodium), retained during the synthesis of the hydrotalcite, could improve the catalytic activity.<sup>[41]</sup> For the citral/MEK reaction, practically no activity was detected when the reaction was carried out over the gas-phase rehydrated catalysts. For the citral/acetone reaction, only 4.5, 5, and 3.5% of citral conversion was observed, even after a reaction period of 23 h, using HT-rg with 29, 39, and 41 wt% of water, respectively. In contrast, over HT-rl, the conversion of citral was 81% in only 5 min. This fact indicates a dramatic difference in the catalytic properties of HT-rg and HT-rl, although characterization of

the samples has indicated the degree of rehydration, which, in principle, should favour the catalyst activity by creation of active OH<sup>-</sup> groups, is higher in HT-rg. Similar differences in performance between HT-rg and HT-rl samples have been observed in the aldol condensation between citral/MEK and the self-condensation reaction of acetone. The conversion of citral over HT-rl was 62% after a reaction period of 3 h. That the citral/MEK reaction is slower than the citral/acetone reaction is attributed to the fact that MEK is larger than acetone as well as the different acidic character of the  $\alpha$ -hydrogen atom in these ketones. For the self-condensation of acetone to DAA using HT-rl as catalyst, the thermodynamic equilibrium (23%) was achieved in less than 0.5 h. Table 4 shows the initial reaction rates for HT-rg,

Table 4. Initial reaction rates and conversion level after 1 h for citral/ketone condensation over HT-rl and HT-rg at 333 K.

Sample	Ketone	Initial rate <sup>[a]</sup> [mmol <sub>citral</sub> g <sub>cat</sub> <sup>-1</sup> h <sup>-1</sup> ]	Conversion of citral [wt %]
HT-rg	acetone	0.41	1
HT-rl	acetone	398.7	97.7
HT-rl-100	acetone	300.8	83.2
HT-rl-700A	acetone	437.5	99.2
HT-rl-700C	acetone	461	99.9
HT-rl	MEK	152.3	49.1

[a] Determined at 5 min of reaction.

and different HT-rl catalysts, used for these aldol condensations at  $T = 333$  K. The data in Table 4 show the beneficial effect of mechanical stirring during the rehydration process. The increase of the surface area of the samples also produces an increase in the catalytic activity. These results confirm that HT-rl samples are more active than HT-rg, accounting on one hand for its greater amount of accessible sites as previously shown. On the other hand, sites of higher strength should be also present, though hardly proved by TPD in CO<sub>2</sub> experiments, because the demanding condensation reaction between citral/MEK only occurs with the samples rehydrated in liquid phase.

**Influence of the reaction temperature:** Previous results for these types of reactions showed that citral was strongly adsorbed on the catalyst surface when working at low temperatures, indicating that a reaction temperature of about 333 K is needed to avoid this undesirable adsorption leading to decreased catalytic activity.<sup>[19]</sup>

In this work, the aldol condensation of citral and acetone was tested at different temperatures (283, 303, and 333 K) over HT-rl. As expected, Figure 13 shows that the reaction took place quickly when the temperature was increased to 333 K (96% of conversion in 30 min), whereas 24 h were necessary for a 91% conversion of citral at 283 K. No change in the product selectivity was observed at the different reaction temperatures studied. An apparent activation energy of 25 kJ mol<sup>-1</sup> was derived from the slope of the Arrhenius plot in Figure 14. This low value for the activation energy could indeed indicate the strong adsorption of the re-

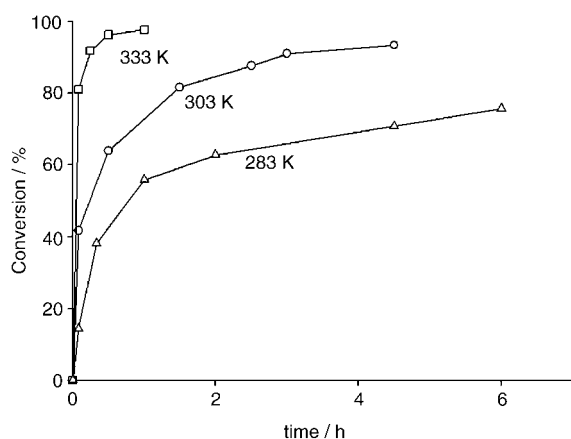


Figure 13. Conversion of citral in the aldol condensation between citral/acetone at different temperatures.

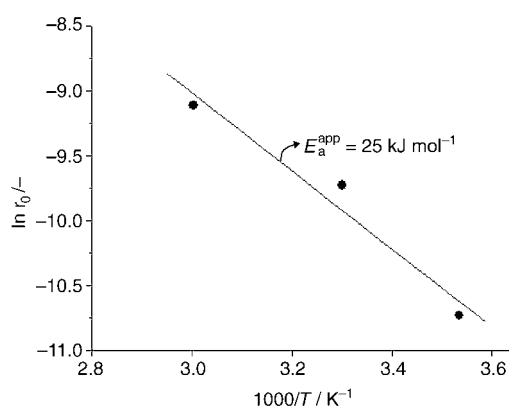


Figure 14. Arrhenius plot of the aldol condensation between citral and acetone over HT-rl.

agents on the catalyst surface. This fact is also confirmed by the brown color acquired for the catalysts at the end of the reaction, even at higher temperatures, instead of the white color in the fresh catalyst.

### Structure–activity relationships

Our results show that basic  $\text{OH}^-$  ions are required in the rehydrated hydrotalcite to obtain high activities in aldol condensation reactions; however, these active  $\text{OH}^-$  are located near the edges of the platelets. This finding supports the suggestion of de Jong and co-workers<sup>[22]</sup> who stated that only 5% of the hydroxy ions of the rehydrated samples are active enough to carry out the reaction. By preparing and testing hydrotalcites with a different platelet size using different ageing conditions,<sup>[40]</sup> we produced a disordered HT structure that increased the basic strength. We then went a step further and customized an enhanced rehydration procedure, first by carrying out the ageing at room temperature and after that, with a liquid-phase rehydration process, with stirring. Consequently, higher surface areas between 200 and  $400 \text{ m}^2 \text{ g}^{-1}$  (depending on the variation of time and the stir-

ring speed during rehydration) were obtained owing to the lower platelet size as well as the porosity within the particles, as supported by microscopy and  $\text{N}_2$  adsorption results. The formation of smaller platelets increases the number of  $\text{OH}^-$  ions near the edges, which contributes more to the enhanced activity. When the rehydration procedure was carried out in the gas phase, the size of the platelets was larger, although the degree of rehydration was higher. Although the  $\text{CO}_2$ -TPD results do not explain the differences in activity because the strength of the  $\text{OH}^-$  groups in HT-rg and HT-rl is similar, not all of the total  $\text{OH}^-$  groups are probed by  $\text{CO}_2$  during the TPD experiments. These  $\text{OH}^-$  groups in the HT-rl samples are more accessible for  $\text{CO}_2$  molecules and for reactants than those in the HT-rg sample.

### Conclusion

This work clearly demonstrates the inactivity of as-synthesized Mg–Al hydrotalcite and the product derived from its thermal decomposition in aldol condensation reactions, and highlights the active nature of Brønsted basic sites in producing superior catalytic performances. To this end, two rehydration procedures were applied to a Mg–Al mixed oxide: in the gas phase (HT-rg) or the liquid phase (HT-rl). TGA, XRD,  $^{27}\text{Al}$  NMR spectroscopy, electron microscopy, and FT-IR analyses show that the rehydration of HT-rg is more efficient than that of HT-rl, with the subsequent higher degree of lamellar structure reconstruction in the former sample. Because the rehydration process leads to a meixnerite-like material that contains Brønsted basic sites ( $\text{OH}^-$ ) in the interlayer spaces, HT-rg samples can be considered to have a higher activity than HT-rl samples in aldol condensation reactions. Nevertheless, HT-rl samples show higher activity than HT-rg samples, indicating that the rehydration method is a crucial step in the activation of the calcined hydrotalcite. Gas-phase rehydration produces a virtually complete reconstruction of the layered structure; however, the final material shows a low specific surface area. This fact means an extreme reduction in the number of exposed active sites owing to a limited accessibility. The specific surface area obtained for the HT-rl samples depends on the rehydration procedure. By increasing the rehydration time and the stirring speed, materials with surface areas approximately 13 and 26 times higher than those of the HT-rg samples are obtained. This fact leads to an increased number of exposed basic sites, and thus to an improved catalytic activity. This is supported by  $\text{CO}_2$ -TPD, which shows that there are more basic sites accessible probed by  $\text{CO}_2$  in HT-rl. We can conclude that the strong difference in surface areas for the two different types of rehydrated samples, the number of basic sites and their accessibility are the main factors for enhancing the catalytic activity of these reactions. Therefore, this provides an approach for the preparation of active catalysts for aldol condensation reactions and, in general, for enhancing the catalytic activity of hydrotalcites by controlling the rehydration process.

## Experimental Section

**Materials:** Mg–Al hydrotalcite (molar Mg/Al ratio = 3:1) was prepared by a coprecipitation method at constant pH ( $10 \pm 0.2$ ) of an aqueous solution of  $\text{Mg}(\text{NO}_3)_2 \cdot 6\text{H}_2\text{O}$  (0.75 M) and  $\text{Al}(\text{NO}_3)_3 \cdot 9\text{H}_2\text{O}$  (0.25 M) and a second solution of  $\text{NaOH}/\text{Na}_2\text{CO}_3$  (2 M). Both solutions were mixed dropwise under stirring at 298 K. After addition of the reactants, the slurry was aged at 298 K for 15 h under vigorous stirring. The precipitate formed was filtered and thoroughly washed with large amounts of deionized water to remove  $\text{Na}^+$  and  $\text{NO}_3^-$  ions. This step is essential because Na impurities can bias the catalytic performance of the rehydrated samples by changing the basic properties of the surface.<sup>[41]</sup> The solid was then dried at 373 K for 18 h to yield the as-synthesized hydrotalcite (HT-as).

The HT-as sample was thermally decomposed in air at 723 K for 15 h to obtain the corresponding Mg–Al mixed oxide (HT-c). This material was rehydrated in both gas and liquid phases. Gas-phase rehydration was carried out by treating the calcined sample in an argon flow saturated with water at room temperature for 15 h ( $40 \text{ mL min}^{-1}$ ) to yield HT-rg (different amounts of water in the sample were also achieved by varying the contact time of the saturated flow (for 10 and 48 h)). Another series of mixed oxides were rehydrated in decarbonated water (1 g of sample in 100 mL of water) for 1 h at room temperature and under mechanical stirring (500 rpm). After the rehydration process, the sample was filtered, washed with ethanol, and dried under argon to yield HT-rl. Some variations in the stirring speed (100, 300 and 700 rpm) and rehydration time (10 min and 5 h) were also performed.

**Methods:** The chemical composition of the samples was determined by ICP-OES in a Perkin-Elmer Plasma 400. The samples were diluted in 10%  $\text{HNO}_3$  before analysis. C,N,H analysis was performed in a Carlo Erba EA1108.

Powder X-ray diffraction patterns were collected in a Siemens D5000 diffractometer with Bragg–Brentano geometry with nickel-filtered  $\text{Cu}_{\text{K}\alpha}$  radiation ( $\lambda = 0.1541 \text{ nm}$ ). Data were collected in the  $2\theta$  range of 5 to 70° with an angular step of 0.05° at 3 s per step, resulting in a scan rate of  $1^\circ \text{ min}^{-1}$ .

$\text{N}_2$  adsorption and desorption isotherms at 77 K were measured on a Quantachrome Autosorb-6B. Prior to analysis, the samples were degassed in vacuum at 393 K for 16 h. The BET, t plot and BJH models (applied to the adsorption branch of the isotherm using cylindrical pore geometry) were used to derive information on the specific surface area, micro- and mesoporosity and pore size distribution, respectively.

Helium pycnometry measurements were performed at 293 K in a Quantachrome pentapycnometer in order to determine the real density of the samples.

Thermal analysis was performed in a Labsys/Setaram TG DTA/DSC thermobalance, equipped with a programmable temperature furnace. The sample (50 mg) was heated from room temperature up to 1173 K in argon ( $80 \text{ cm}^3 \text{ STP min}^{-1}$ ) at  $5 \text{ K min}^{-1}$ .

Infrared spectra were recorded on a Bruker-Equinox-55 FTIR spectrometer. The spectra were acquired by accumulating 64 scans at  $4 \text{ cm}^{-1}$  resolution in the range of 400–4000  $\text{cm}^{-1}$ . Samples were prepared by mixing the powdered solids with pressed KBr disks (blank) in a ratio of 15:85. The different samples were stored under argon to avoid absorption of  $\text{CO}_2$ . The calcined sample was analyzed in flowing Ar at 723 K in an in-situ cell with the diffuse reflectance (DRIFT) mode.

Scanning electron microscopy images were recorded at 5 kV in a JEOL JSM-6700F field-emission microscope. Samples were coated with palladium to create contrast.

Transmission electron microscopy was carried out on a Philips CM30UT electron microscope with a field emission gun as the source of electrons operated at 300 kV. Samples were mounted on Quantifoil carbon polymer supported on a copper grid by placing a few droplets of a suspension of the ground sample in ethanol on the grid, followed by drying at ambient conditions.

$^{27}\text{Al}$  MAS-NMR experiments were performed at 9.4 T on a Varian VXR-400S spectrometer operating at 104.2 MHz with a pulse width of 1 ms.

The narrow bore magnet (50 mm) was fitted with a high-speed magic angle spinning (MAS) Doty probe. The samples were spun in 4 mm zirconia rotors with a spinning frequency of 8 kHz. A total of 4000 scans were collected with a sweep width of 100 kHz and an acquisition time of 0.2 s. An acquisition delay of 1 s between successive accumulations was selected to avoid saturation effects. The  $^{27}\text{Al}$  chemical shifts were referenced to  $[\text{Al}(\text{H}_2\text{O})_6]^{3+}$ .

The basic properties of the samples were determined by TPD of  $\text{CO}_2$  in a Thermo Finnigan TPDRO1100 equipped with a programmable temperature furnace and a TCD detector. The gas outlet was coupled to a quadrupole mass spectrometer Pfeiffer GSD300. A method similar to that of Padmasri et al.<sup>[42]</sup> was applied. Typically,  $\approx 100 \text{ mg}$  of solid was placed between quartz wool in a quartz reactor, pre-treated in argon at 373 K for 1 h, and then cooled to 353 K, prior to the adsorption of  $\text{CO}_2$  at this temperature. After adsorption of  $\text{CO}_2$  (3 vol.%  $\text{CO}_2$  in He;  $20 \text{ cm}^3 \text{ STP min}^{-1}$ ) for 60 min, the catalyst was treated in He ( $20 \text{ cm}^3 \text{ STP min}^{-1}$ ) for 45 min at 373 K to remove the physically adsorbed  $\text{CO}_2$ . The  $\text{CO}_2$  uptake was measured by treating the sample from room temperature up to 1173 K at a heating rate of  $10 \text{ K min}^{-1}$  and recording the results with a TCD detector. Peak deconvolution was performed by using the software of the equipment, and the number of Brønsted basic sites was determined assuming that one molecule of  $\text{CO}_2$  adsorbs on each basic site.

**Catalyst testing:** Aldol condensation reactions were performed in a 100-mL round-bottom flask equipped with a magnetic stirrer and a condenser system in argon under  $\text{CO}_2$ -free conditions. For a typical reaction between citral (40.8 mmol) and ketone (180 mmol), a ketone/citral ratio of 4.4:1 was used. This solution was stirred at the desired temperature and 1 g of catalyst was added. The reaction was carried out in the range of 283–333 K. For the self-aldol condensation of acetone (0.25 mol), 1 g of catalyst was also used and the reaction was conducted at 273 K. Samples were taken at regular time intervals and were analysed off-line by gas chromatography (GC) using a FID detector and an ULTRA2 column ( $15 \text{ m} \times 0.32 \text{ mm} \times 0.25 \mu\text{m}$ ). Tetradecane was used as the internal standard. Citral, pseudoionone, acetone (95%) and 2-butanone (MEK) were purchased from Aldrich and were used without further purification.

## Acknowledgement

This work has been financially supported by the Ministerio de Ciencia y Tecnología of Spain (REN2002-04464-CO2-01, PETRI 95-0801.OP) and Destilaciones Bordas S.A. Dr. P. J. Kooyman (TU Delft), K. Djanashvilli (TU Delft), and T. Bach (Hydro) are acknowledged for performing the TEM,  $^{27}\text{Al}$  MAS-NMR, and SEM studies, respectively.

- [1] F. Cavani, F. Trifiro, A. Vaccari, *Catal. Today* **1991**, *11*, 173.
- [2] V. R. L. Constantino, T. J. Pinnavaia, *Inorg. Chem.* **1995**, *34*, 883.
- [3] J. I. Di Cosimo, V. K. Díez, M. Xu, E. Iglesia, C. R. Apesteguía, *J. Catal.* **1998**, *178*, 499.
- [4] D. Tichit, B. Coq, *CATTECH* **2003**, *7*, 206.
- [5] Y. Ono, *J. Catal.* **2003**, *216*, 406.
- [6] W. T. Reichle (Union Carbide Corporation), US 4476324, **1984**.
- [7] G. Zhang, H. Hattori, K. Tanabe, *Appl. Catal.* **1988**, *36*, 189.
- [8] D. Tichit, M. N. Bennani, F. Figueras, R. Tessier, J. Kervennal, *Appl. Clay Sci.* **1998**, *13*, 401.
- [9] D. Tichit, B. Coq, S. Cerneaux, R. Durand, *Catal. Today* **2002**, *75*, 197.
- [10] M. J. Climent, A. Corma, V. Fornés, R. Guil-Lopez, S. Iborra, *Adv. Synth. Catal.* **2002**, *344*, 1090.
- [11] K. K. Rao, M. Gravelle, J. Sánchez-Valente, F. Figueras, *J. Catal.* **1998**, *173*, 115.
- [12] M. L. Kantam, B. M. Choudary, C. V. Reddy, K. K. Rao, F. Figueras, *Chem. Commun.* **1998**, *9*, 1033.
- [13] M. J. Climent, A. Corma, S. Iborra, J. Primo, *J. Catal.* **1995**, *151*, 60.
- [14] A. Guida, M. H. Lhouty, D. Tichit, F. Figueras, P. Geneste, *Appl. Catal. A* **1997**, *164*, 251.

- [15] B. M. Choudary, M. L. Kantam, C. R. V. Reddy, K. K. Rao, F. Figueras, *J. Mol. Catal. A* **1999**, *146*, 279.
- [16] T. Hibino, A. Tsunashima, *Chem. Mater.* **1998**, *10*, 4055.
- [17] N. S. Puttaswamy, P. Vishnu Kamath, *J. Mater. Chem.* **1997**, *7*, 1941.
- [18] M. J. Climent, A. Corma, S. Iborra, A. Velty, *Catal. Lett.* **2002**, *79*, 157.
- [19] M. J. Climent, A. Corma, S. Iborra, A. Velty, *Green Chem.* **2002**, *4*, 474.
- [20] J. C. A. A. Roelofs, A. J. van Dillen, K. P. de Jong, *Catal. Lett.* **2001**, *74*, 91.
- [21] J. C. A. A. Roelofs, A. J. van Dillen, K. P. de Jong, *Catal. Today* **2000**, *60*, 297.
- [22] J. C. A. A. Roelofs, D. J. Lensveld, A. J. van Dillen, K. P. de Jong, *J. Catal.* **2001**, *203*, 184.
- [23] F. Figueras, J. López, J. Sánchez-Valente, T. T. H. Vu, J.-M. Clacens, J. Palomeque, *J. Catal.* **2002**, *211*, 144.
- [24] J. Sánchez-Valente, F. Figueras, M. Gravelle, P. Khumbar, J. López, J.-P. Besse, *J. Catal.* **2000**, *189*, 370.
- [25] J. López, R. Jacquot, F. Figueras, *Stud. Surf. Sci. Catal.* **2000**, *130*, 491.
- [26] A. Morato, C. Alonso, F. Medina, Y. Cesteros, P. Salagre, J. E. Sueiras, D. Tichit, B. Coq, *Appl. Catal. B* **2001**, *32*, 167.
- [27] F. Prinetto, G. Ghiotti, P. Graffin, D. Tichit, *Microporous Mesoporous Mater.* **2000**, *39*, 229.
- [28] J. Pérez-Ramírez, G. Mul, F. Kapteijn, J. A. Moulijn, *J. Mater. Chem.* **2001**, *11*, 821.
- [29] J. T. Klopogge, R. L. Frost, *Phys. Chem. Chem. Phys.* **1999**, *1*, 1641.
- [30] F. Prinetto, G. Ghiotti, R. Durand, D. Tichit, *J. Phys. Chem. B* **2000**, *104*, 11117.
- [31] J. T. Klopogge, R. L. Frost, *Appl. Catal. A* **1999**, *184*, 61.
- [32] F. Millange, R. I. Walton, D. O'Hare, *J. Mater. Chem.* **2000**, *10*, 1713.
- [33] W. Yang, Y. Kim, P. K. T. Liu, M. Sahimi, T. Tsotsis, *Chem. Eng. Sci.* **2002**, *57*, 2945.
- [34] N. N. Greenwood, A. E. Earnshaw, *Chemistry of the elements*, Pergamon Press, New York, **1984**, p. 329.
- [35] J. Shen, M. Tu, C. Hu, *J. Solid State Chem.* **1998**, *137*, 295.
- [36] J. I. Di Cosimo, C. R. Apesteguía, M. J. L. Ginés, E. Iglesia, *J. Catal.* **2000**, *190*, 261.
- [37] M. A. Aramendía, V. Borau, C. Jiménez, J. M. Marinas, J. R. Ruiz, F. J. Urbano, *Appl. Catal. A* **2003**, *255*, 301.
- [38] V. K. Díez, C. R. Apesteguía, J. I. Di Cosimo, *J. Catal.* **2003**, *215*, 220.
- [39] A. Alejandre, F. Medina, X. Rodríguez, P. Salagre, J. E. Sueiras, *J. Catal.* **1999**, *188*, 311.
- [40] W. T. Reichle, *J. Catal.* **1985**, *94*, 547.
- [41] S. Abelló, F. Medina, D. Tichit, J. Pérez-Ramírez, X. Rodríguez, J. E. Sueiras, P. Salagre, Y. Cesteros, *Appl. Catal. A* **2004**, in press.
- [42] A. H. Padmasri, A. Venugopal, V. Durga Kumari, K. S. Rama Rao, P. Kanta Rao, *J. Mol. Appl. Catal. A* **2002**, *188*, 255.

Received: April 27, 2004  
Published online: December 6, 2004